國立臺灣大學工學院化學工程學研究所

碩士論文

Department of Chemical Engineering
College of Engineering
National Taiwan University
Master Thesis

基於氣相聚合與熱裂解製程的多層級孔洞碳材

Hierarchical and Porous Carbon Structures Based on Vapor-Phase Polymerization and Pyrolysis Process

吳易倡

Yi-Chang Wu

指導教授：陳賢燁 博士

Advisor: Hsien-Yeh Chen, Ph.D.

中華民國 112 年 6 月

June, 2023

doi:10.6342/NTU202301165

國立臺灣大學碩士學位論文
口試委員會審定書

基於氣相聚合與熱裂解製程的多層級孔洞碳材
Hierarchical and Porous Carbon Structures Based on Vapor-Phase Polymerization and Pyrolysis Process

本論文係吳易倡君（r10524044）在國立臺灣大學化工學系、所完成之碩士學位論文，於民國 112 年 6 月 21 日承下列考試委員審查通過及口試及格，特此證明

口試委員：陳貴婷（簽名）

（指導教授）

陳柏均　　許子衿

系主任、所長 廖英志（簽名）

（是否須簽章依各院系所規定）

doi:10.6342/NTU202301165

摘要

隨著全球暖化問題日益嚴重，綠色環保意識逐漸提升，能源儲存、氣體吸附與電化學催化等研究領域正在蓬勃發展，其中碳材扮演著不可或缺的角色。在本篇研究中，以氣相聚合的製程形成多層級孔洞高分子材料，並經過高溫將聚對二甲苯高分子碳化，其形貌因為添加矽酸鹽類仍能維持，成功合成多級孔洞碳材結構。

傳統製造孔洞碳材為硬模板方法，與傳統方法不同的是，此新穎製程為具有較大孔徑的孔洞碳材提供了一條快速合成且綠色化學的合成路徑。此多層級孔洞是來自於暫時的泡沫狀冰塊模板進行化學氣相沉積，因被空氣體積佔據形成的泡沫空腔形成了約數百微米至公分級的一級孔洞；另一方面，泡沫支架經歷了冷凍乾燥機制，形成了約數十微米大小的次級孔洞；此多層級孔洞材料經歷熱裂解製程之後，氣相聚合在矽酸鹽框架上的保形高分子薄膜進而被碳化成碳膜。為了強調這種製程使材料形貌有高度可調性，我們利用具有分形結構的樣品作為演示。此外，本研究設計一項絕熱效果實驗，其數據顯示這種泡沫狀多層級孔洞碳材具有出色的絕熱效果。

關鍵詞: 氣相沉積；碳材；多級孔洞；絕熱效果

doi:10.6342/NTU202301165

Abstract

As the issue of global warming grows more severe, the importance of green environmental consciousness is on the rise. Research fields such as energy storage, gas adsorption, and electrochemical catalysis are seeing rapid development, with carbon materials playing an essential role in these areas. In this study, a hierarchical porous polymer material was formed through gas-phase polymerization and carbonized at high temperature to yield a hierarchically porous carbon structure that maintained its morphology due to the addition of silicate. Differing from the encapsulation of solid materials using methods like the hard-template approach, this novel fabrication process provides a time-efficient and eco-friendly synthesis route for porous carbon with larger pore sizes. It was from the CVD process of temporal foam-like ice-template. The cell window was from the original occupied space of air volume, forming primary pore sizes from approximately 100 micrometers to centimeters. On the other hand, the strut underwent a freeze-drying process, resulting in the formation of a secondary pore structure with pore sizes around 10 micrometers. There is a conformal carbon film on the framework of laponite due to the carbonization of dense parylene film coating. To emphasize the characteristics of highly tunable morphology of this approach, we presented a sample with fractal structure, showing their potential for various application. Moreover, a straightforward thermal insulation test indicated the excellent thermal insulation performance of this foam-like carbon structure.

Keywords: Vapor-phase polymerization, carbon material, hierarchical porous structure, thermal insulation performance

doi:10.6342/NTU202301165

Content

摘要 I

Abstract II

Content III

List of Figures V

Chapter 1 Introduction 1

1.1 Classification of Carbon-based materials 1

1.2 Porous Carbon 3

1.3 Hierarchical Porous Carbon 6

1.4 Chemical Vapor Polymerization 7

Chapter 2 Experimental 9

2.1 Characterizations 9

2.1.1 Thermogravimetric analysis (TGA) 9

2.1.2 Raman spectroscopy 9

2.1.3 X-ray diffraction 9

2.1.4 Scanning electron microscopy (SEM) 10

2.1.5 3D profile microscope 10

2.1.6 Nitrogen adsorption-desorption isotherm (BET) 10

2.1.7 Atomic force microscope (AFM) 10

2.2 Temporal bubble structures 11

2.3 Vapor phase polymerization and water sublimation process 12

Chapter 3 Results and Discussion 13

doi:10.6342/NTU202301165

3.1 Carbonization process 13
3.1.1 Material characterizations 15
3.1.2 Morphology change 18
3.2 Structural integrity improvement 21
3.3 Hierarchical porous structure 23
3.3.1 Hierarchy structure 23
3.3.2 Tunable morphology of foam-like structure 26
3.3.3 Thermal insulation test 28
Chapter 4 Conclusion 31
4.1 Conclusion 31
4.2 Future work 32
Reference 34
Appendix 39

doi:10.6342/NTU202301165

List of Figures

Figure 1.1 Concept illustration of hard template method. 5

Figure 2.1 Schematic illustration of temporal bubble structures with different sizes. ... 11

Figure 3.1 Illustration of coking and charring mechanism. 14

Figure 3.2 Thermogravimetric curve of parylene C. 15

Figure 3.3 Raman spectrum of parylene C (a) before carbonization and (b) after carbonization. 16

Figure 3.4 XRD results of parylene C (a) before carbonization and (b) after carbonization. 17

Figure 3.5 Thickness of dense film coating parylene (a) before carbonization and (b) after carbonization, measured with AFM. 18

Figure 3.6 SEM images for (a) porous parylene before carbonization and (b) porous carbon from porous parylene after carbonization. 19

Figure 3.7 3D profile imaging of (a) porous parylene with foam structure before carbonization and (b) porous carbon from porous parylene with foam structure after carbonization. (addition of 0.1 wt% tween80) 20

Figure 3.8 SEM of cross-section view of (a) porous parylene before carbonization and (b) porous carbon from porous parylene after carbonization. (addition of 1 wt% laponite) 22

Figure 3.9 Raman spectrum and SEM of top view of porous carbon from porous parylene after carbonization. (addition of 1wt% laponite) 22

Figure 3.10 (a) Schematic representation of the hierarchical foam-like porous carbon structure. (b) Illustration of tunable primary pore size and structural integrity showed by SEM images. (addition of 0.1 wt% tween80 and 2% wt% laponite) 25

doi:10.6342/NTU202301165

Figure 3.11 Tunable morphology illustration by fractal foam structure. (addition of 0.1 wt% tween80 and 2% wt% laponite) 27
Figure 3.12 (a) Schematic illustration of thermal insulation experiment setup. (b) Time required for completely melting of ice for the control, PDMS and fractal bubble structure carbon. (c) Comparison of time required for completely melting of ice between foam-like porous structure and freeze-drying derived porous structure, with the examination of the impact of carbonization process. 30
Figure 4.1 BET surface area of pristine laponite and laponite annealed at 850°C. 33

doi:10.6342/NTU202301165

Chapter 1 Introduction

1.1 Classification of Carbon-based materials

Research about carbon-based materials are getting much more attention recently. There are several advantages of carbon-based materials, for example, its characteristic of lightweight and strong mechanical properties. Moreover, it has excellent electric conductivity and thermal conductivity, which may replace the role of metal. When it comes to carbon-based materials, there are two opinions to comprehend these materials. One is on the basis of electron hybridized orbitals[1]. Allotropes of carbon like diamond, graphite and carbyne, are corresponding to sp^3, sp^2, sp hybridization respectively. Diamond structure has completely sp^3 hybridization, whose four electrons are satisfied, resulting the insulating electric property, good thermal conductivity and hardness[2]. Graphite is composed of multi-layer graphene, and each graphene layer is a flat hexagonal crystalline structure with sp2 bonds[3]. Graphene, by definition, is a two-dimensional material with only one carbon atom layer. Its appealing characteristics of transparent optical properties and high thermal conductivity makes it a highly potential role in application. Carbyne is the ideal carbon material with infinite chain structure, which has sp hybridized orbital. However, this material is still full of controversies[4]. Besides, fullerenes, whose molecular nanostructures have curvature, are carbon materials with sp^2 hybridized orbital. For example, carbon nanotube and buckyball are fullerenes. The main difference between fullerenes and graphene is that the former has nanostructure of spherical cage-like, not sheet-like[5]. There is a theory, pyramidalization, explaining the curvature-induced change in hybridization[5]. As a result, we can regard fullerenes as

doi:10.6342/NTU202301165

carbon materials with sp^{2+n} hybridized orbital.

Rather than on the view of hybridization of electron orbitals, the other opinion to comprehend carbon material is on the view of molecular nanostructure. For example, graphene quantum dot[6] and buckyball, C_{60} are zero-dimensional nanomaterial. Carbon nanotube and carbon nanofiber are one-dimensional nanomaterial[7]. Carbon sheet and graphene are two-dimensional carbon-based material[8]. Last but not least, porous carbon and 3D graphene are three-dimensional materials[9], which are usually seen in many applications such as energy storage and energy conversion[10]. Strictly speaking, graphene is an ideal material with only one carbon atom layer. In the literature[11], it gives a detailed definition and recommended nomenclature for graphene-based material. Multi-layer graphene is composed of 2~10 layers of well-defined stacked graphene. Carbon films with uncountable number of layers of carbon atom (> 10 layers graphene) or discontinuous stacking order of graphene layer should be called "carbon thin films"[11].

doi:10.6342/NTU202301165

1.2 Porous Carbon

Porous carbon refers to carbon materials with microscopic or macroscopic pore size. Undoubtedly, research about porous carbon is getting important in these days. Porous carbon materials have characteristics of high specific surface area, lightweight, excellent thermal conductivity and good electrical properties, so they can be applied in energy storage, gas storage, water treatment and batteries research field[12]. Porous carbon can be made from many kinds of fabrication routes[13], which can be divided into template-assisted method and template-free method. Template-assisted method involves hard template, soft template and self-template. The concept of template-assisted method[14] contains the following steps: (1) the occupied space due to a template. (2) introduction of carbon source (polymer) on the template via by wet impregnation or polymerization. (3) direct carbonization of carbon source. (4) removal of the template. Take hard template method for example, which is shown in Figure 1.1. Hard template is usually inorganic materials like silica, metal oxide, and zeolite[15]. The porous carbon structure is a negative replica of hard template, so the pore size can be tuned by choosing different particle size of inorganic material. However, there is usually the participation of strong acid or strong base etching agents during the removal of hard template. In contrast, soft template method is advantageous for its easier removal template during pyrolysis, but it is time-consuming for the reactions between carbon source and surfactants[16]. Self-template method can be from biomass material or metal-organic framework (MOF) acting as templates. The biomass precursor would have pore formation during pyrolysis process[17]. However, it is usually required for an activation process. Activation of carbon is a useful way to produce micropores[18]. The main disadvantage of biomass-derived porous carbon is because of intrinsic pore structure, which is hard to control pore size.

doi:10.6342/NTU202301165

One of template-free method is sol-gel controlling. Take carbon aerogels as example, the classical and conventional fabrication process contains three steps: polymerization, drying, and carbonization[19]. Usually, scientists use gelation reaction to get cross-linked polymer material. The polymerization often takes place in the liquid phase solution. After the polymerization, there is a needed drying process to evaporate the solvent. Followed by the next step, this polymer conducts pyrolysis process to carbonize the polymer into carbon. The porosity, pore size distribution and texture properties could be customized by different preparation conditions, such as pH, temperature and ageing time[20].

The above introduced methods can briefly and roughly give explanation about pore formation mechanism of porous carbon materials. However, the research about carbonization process itself is also important. For example, there would be morphology change or thermal stability problem of templates. Besides, the carbonization process parameters would depend on the type of polymer. There will be a further detailed discussion about carbonization in the “Results and Discussion part”.

doi:10.6342/NTU202301165

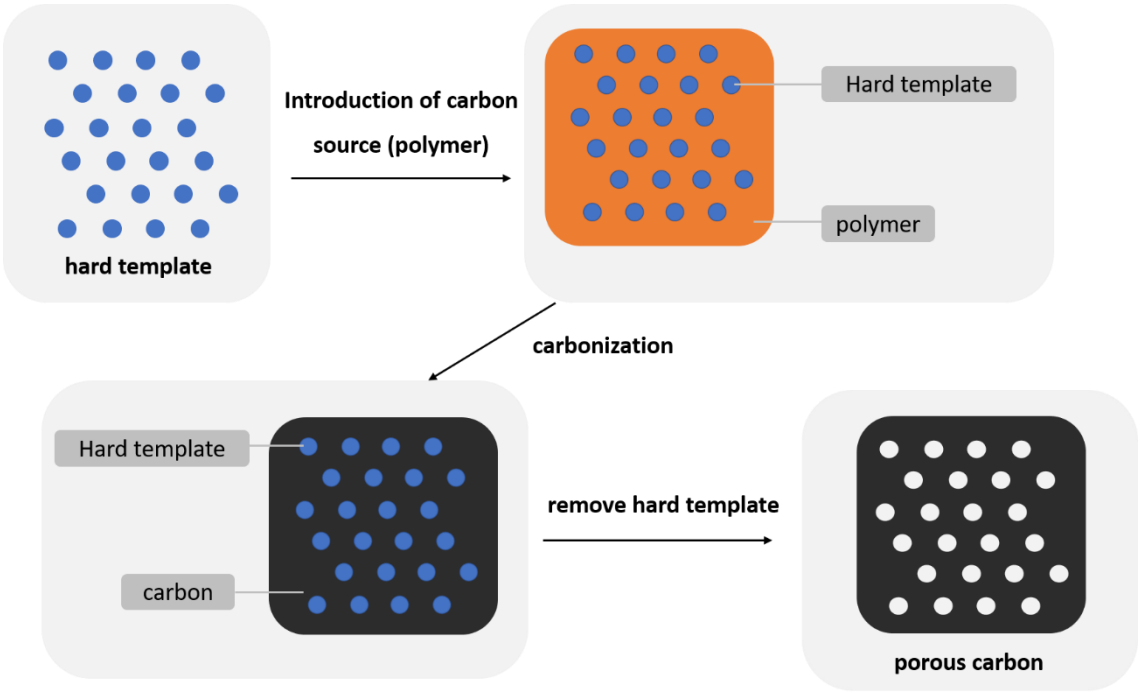

Figure 1.1 Concept illustration of hard template method.

doi:10.6342/NTU202301165

1.3 Hierarchical Porous Carbon

In material science, controlling the pore size distribution of a material is challenging for scientists, no matter what in which research field. By definition, one can classify the pore size into three types, micropores (pore diameter less than 2 nm), mesopores (pore diameter between 2 nm and 50 nm) and macropores (pore diameter larger than 50 nm). With synergy effect of these three distinct pore sizes at different scales, hierarchical porous carbon can enhance the electrochemical performance. For example, micropores can supply lots of surface area and active sites for ion storage. Mesopores are able to facilitate the mass transport pathways for ions. Macropores can minimize the diffusion distance of ions, acting like the ion-buffer reservoirs[21].

In fact, for supercapacitor application or electrochemical catalysis, the effective specific surface area is indeed the key factor that determine the fundamental performance[22]. High specific surface area is due to the presence of micropores. However, the presence of micropores does not guarantee well performance since that some micropores are inaccessible to the electrolyte ions. As a result, the hierarchical pore structure contributes a synergy effect, combining the advantages of each pore size scale. The hierarchical structure design can not only be bimodal at a single scale length but also span across two or three length scales such as mirco-meso, micro-macro,meso-macro or even micro-meso-macro levels[13]. Besides pores at different length scales, whether the pore structures are in order and the geometric of pore shape also cause influence in diffusion behaviors of electrolyte.

doi:10.6342/NTU202301165

1.4 Chemical Vapor Polymerization

Poly-para-xylene, also called parylene, is a unique polymer material not only from its polymerization mechanism but also its characteristics of physical and chemical properites. Parylene has been a commercial polymer material, applied in many applications and researches. Chemical-inert is one of its advantages, making it as a chemical protection barrier for electronic components. Parylene also acts as good thermal and electric insulation layer[23], and its biocompatibility makes it a suitable encapsulation layer of biomedicals[24]. Moreover, parylene is famous for the conformal coating ability, making itself a special and vital role in lots of application[25].

In 1966, Gorham proposed a novel synthetic method of parylene[26]. The Gorham process can be divided into three steps: sublimation of dimer, pyrolysis into monomer, polymerization into polymer. First, the precursor, paracyclophane, would be put in the vacuum vessel and heated at around 100˚C to sublimate into gas phase. This gas phase dimer would be transported by inert gas to the furnace. Typically, 650˚C condition is enough to pyrolyze the dimer into monomer. Each monomer is a highly reactive radical. Next, the monomer would continually be transported by inert gas into deposition chamber. The monomer needs to adsorb on the substrate then be able to start polymerization. According the theory proposed by Fortin[27], there is a well control of polymerization rate by adjusting the substrate temperature and monomer concentration in the deposition chamber. It is worth to note that the polymerization rate is faster at lower temperature, which is favored with physical adsorption of monomer.The whole process has no by-product, and deposition of parylene is a dry process at room temperature. Moreover, based on the proposed mechanism of water vapor sublimation and parylene monomer deposition[28], it is simply to fabricate an interconnected porous structure from ice-template.

doi:10.6342/NTU202301165

The sublimation rate of ice-template is the rate determined state of adjusting pore size distribution[29]. As a result, tunable pore size is achievable.

In conclusion, this vapor phase polymerization has several advantages and significant characteristics: (1) excellent control of ultra-thin parylene film coating thickness[30] and conformality, which is highly potential to develop a new fabrication method of 3D graphene. (2) couple hours of reaction time. (3) green process to generate pore structure, no involvement of toxic chemicals and etching agent. Herein we demonstrated parylene as the precursor of carbon source to fabricate porous carbon structures. Thanks to the successful replacement of ice-template into porous parylene structure and carbonization process, we can fabricate hierarchical porous carbon with an easier way.

doi:10.6342/NTU202301165

Chapter 2 Experimental

2.1 Characterizations

2.1.1 Thermogravimetric analysis (TGA)

Poly(2-chloro-p-xylylene), also called parylene C was analyzed with SDT650 (TA instruments, USA) to know the weight change during pyrolysis process. The whole process was conducted in nitrogen atmosphere. The ramping process was 10˚C/min to 300˚C, and then changed to 5˚C/min to 850˚C. Last, the temperature was held at 850˚C for an hour to make sure the carbonization process almost complete.

2.1.2 Raman spectroscopy

The Raman spectra were collected using an inVia^{TM} confocal microscope (Renishaw, UK) with He-Ne laser for 633 nm excitation. The spectra were smoothed and baseline subtracted with Renishaw WiRE 5.0 software. The measurements were carried out with 10 seconds exposure time and 10% power intensity. Each Raman spectrum showed the intensity versus Raman shift, ranging from 600 cm^{-1} to 3400cm^{-1}.

2.1.3 X-ray diffraction

The X-ray diffraction spectra were collected with X-ray diffractor (Rigaku SmartLab^{R}, Japan) to analyze the crystalline structure of materials. All the measurements used copper (Cu) Kα to generate X-ray source. Each sample was measured with scanning speed 5 ˚C/min, ranging from 10˚ to 60˚. The datas were smoothed and plot with OriginLab software. The baseline was subtracted

doi:10.6342/NTU202301165

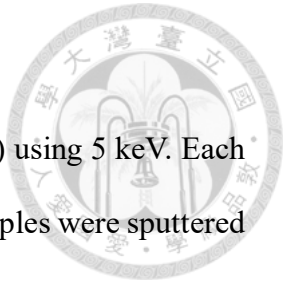

2.1.4 Scanning electron microscopy (SEM)

SEM imaging was captured with Nova^{TM} NanoSEM (FEI, USA) using 5 keV. Each sample was put in the vacuum at room temperature overnight. All samples were sputtered with platinum for 4 minute with a current of 20 mA.

2.1.5 3D profile microscope

The foam-like structures were captured with VK-9500 3D profile microscope (Keyence, Japan).

2.1.6 Nitrogen adsorption-desorption isotherm (BET)

The specific area and pore size distribution was measured with nitrogen gas adsorption method. The instrument was Micrometrics ASAP2010. The degas temperature was 200˚C. Before measurement, samples were put in the 110˚C oven in the vacuum overnight.

2.1.7 Atomic force microscope (AFM)

The thickness of parylene film and carbon sheet was measured with Bruker AFM. The morphology was pictured with NanoWorld AFM tips using tapping mode. By scratching the film surface with the tip of a needle, there was a height difference produced between the height level of wafer and film. This height difference was regarded as the basis of thickness.

doi:10.6342/NTU202301165

2.2 Temporal bubble structures

Bubble structures were created by the bubble blowing process. At the beginning, 0.1 wt% solution of tween80 (Sigma) was prepared. Due to the addition of surfactant agent, the liquid solution would form bubbles easily as the gas was injected to the liquid. In this research, there were two ways to produce bubbles with different sizes, as shown in Figure 2.1. Intuitively, one way was to use the pipette filled with air and push the plunger slowly to inject it into bubbles. This kind of blowing process was appropriate for fabricating centimeter scale of bubble pore diameter and countable numbers of bubble. Alternatively, the other way was to use the tools like milk frother to do agitation in the liquid. This method produced numerous bubbles, whose pore sizes were in the range of hundreds of micrometers. The bubbles would burst because of the evaporation of water on the bubble surface or the disruption of surface tension. Therefore, the bubble structures would be frozen into ice-template with liquid nitrogen bath (LNG) below as a cooling agent to maintain integrity of the structure.

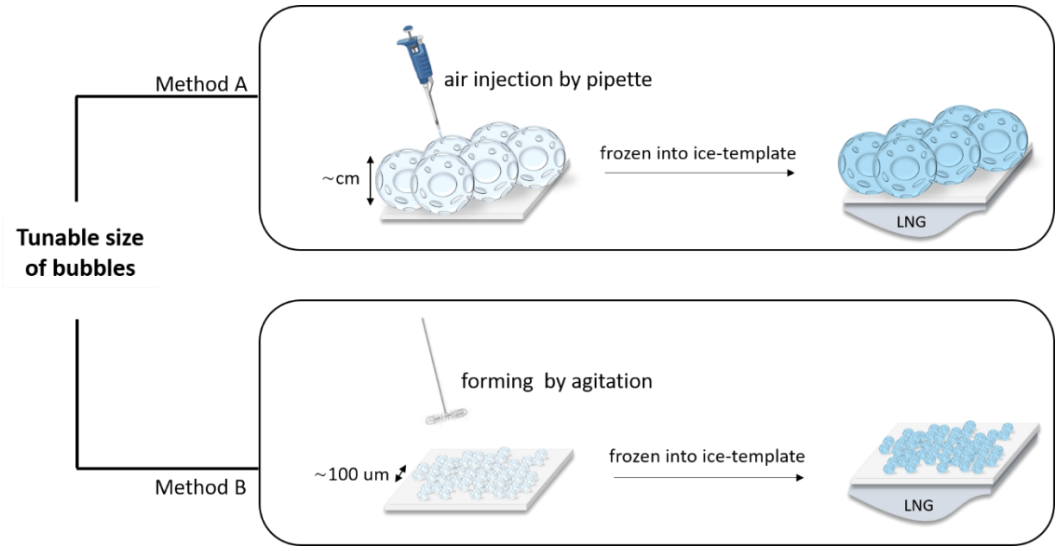

Figure 2.1 Schematic illustration of temporal bubble structures with different sizes.

doi:10.6342/NTU202301165

2.3 Vapor phase polymerization and water sublimation process

The adjustable experimental parameters of custom-built vacuum system were divided into three parts: (1) flowing rate of inert gas. (2) temperature of dimer. (3) temperature of cooling plate. For substrate with ice-template on it, the cooling temperature was set to be 0°C to control the sublimation rate of ice. At the beginning of vacuuming, the dimer was away from pyrolysis furnace as far as possible to avoid parylene from polymerizing on the frost of ice. The flow of argon was turned off also for the same purpose. After several minutes, flow rate of argon was changed to 5 sccm and dimer was put at the location of which temperature was about 50°C. The whole process finished until the system back to its base pressure.

For substrate with no ice-template on it, the cooling temperature was set to be 25°C. The flow of argon was 5 sccm consistently and dimer was put at the location of which temperature was about 50°C. The whole process finished until the system back to its base pressure.

doi:10.6342/NTU202301165

Chapter 3 Results and Discussion

3.1 Carbonization process

There are two synthesized routes for carbon-based materials, bottom-up and top-down, respectively. Chemical vapor deposition (CVD) and Plasma-enhanced CVD are examples of bottom-up fabrication method of carbon materials. However, this method usually contains the participation of metal catalyst, which may cause contamination or decreased quality of graphene when graphene transfer process[31]. Carbonization, which is the process during pyrolysis of organic polymer into carbon, is one of top down methods. For example, carbon microelectromechanical system (C-MEMS) has been a promising technologies for biosensors and energy storage[32]. Scientists in this research field have demonstrated direct pyrolysis of patterned photoresist SU-8 microstructure into carbon microsupercapacitors[33].

Generally, carbonization is the thermochemical decomposition of organic materials in the absence of oxygen. As a result of carbon backbone of polymer, it always yields some non-volatile carbon. Depending on the pyrolysis condition like ramping rate, pressure, atmosphere gas and the type of polymer, the purity of carbon may vary. Typically, the carbonization temperature is around 850°C. The carbon would start graphitization if the temperature is higher than 2000°C. Graphitization makes amorphous carbon have crystalline structure, resulting its increasing graphitization degree[34] and better thermal conductivity and electrical properties. However, it is inevitable to occur shrinkage of morphology during carbonization process[35]. In fact, the polymer-derived carbon may come from two potential carbonization mechanisms, coking and charring, respectively[36]. Figure 3.1 provides a visual illustration of the key distinction between

doi:10.6342/NTU202301165

coking and charring. Basically, coking refers to the polymer passing through a liquid or semi-solid state at once during carbonization, trying to minimize surface energy. Charring refers to the polymer structure (skeleton) remains rigid but existence of pores[37]. Generally, both of these two phenomena are results of volatile hydrocarbon gas accompanied with carbonization process. In other words, there is a net mass loss from the organic material, which leads to the shrinkage (coking) or porosity (charring). Consequently, we do the following material characterizations and surface imaging techniques to comprehend what happened to parylene during the carbonization process.

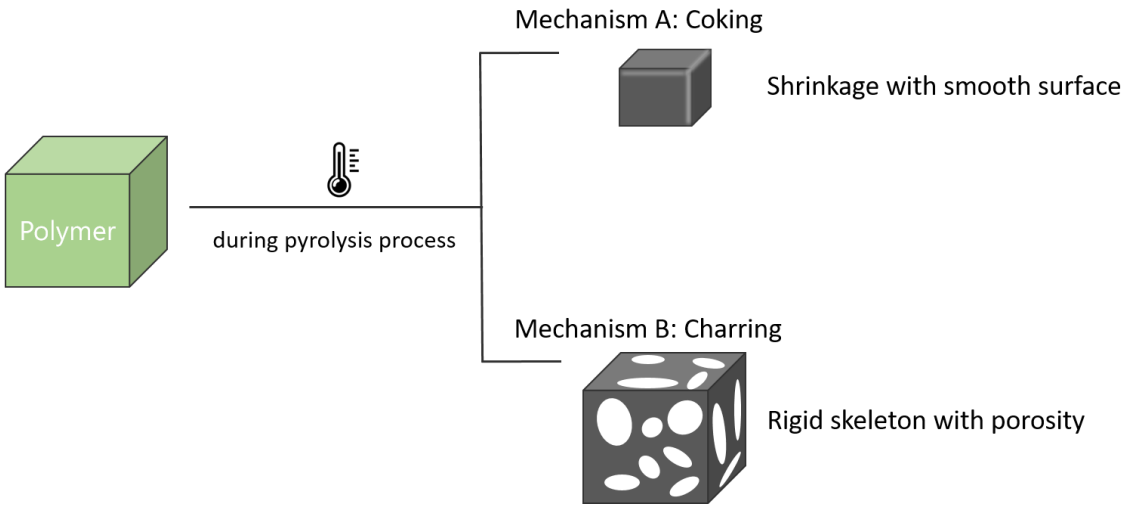

Figure 3.1 Illustration of coking and charring mechanism.

doi:10.6342/NTU202301165

3.1.1 Material characterizations

At the beginning, we did thermogravimetric analysis (TGA) to make sure the carbonization process happened. Figure 3.2 was the thermogravimetric curve of parylene C. As a result of hydrophobicity of parylene C, it was not obvious to see weight change during 100˚C to 200˚C due to adsorption of water molecule on itself. It apparently showed that weight of parylene C had a suddenly dramatic drop around 500˚C, which was consistent with the reference[38]. This environment temperature gave enough energy for breaking C-H bonds[39], resulting weight loss in the form of hydrocarbon gas. To confirm the pyrolysis process was finished, we elevated the heating temperature to 850˚C and keeping isothermal for an hour.

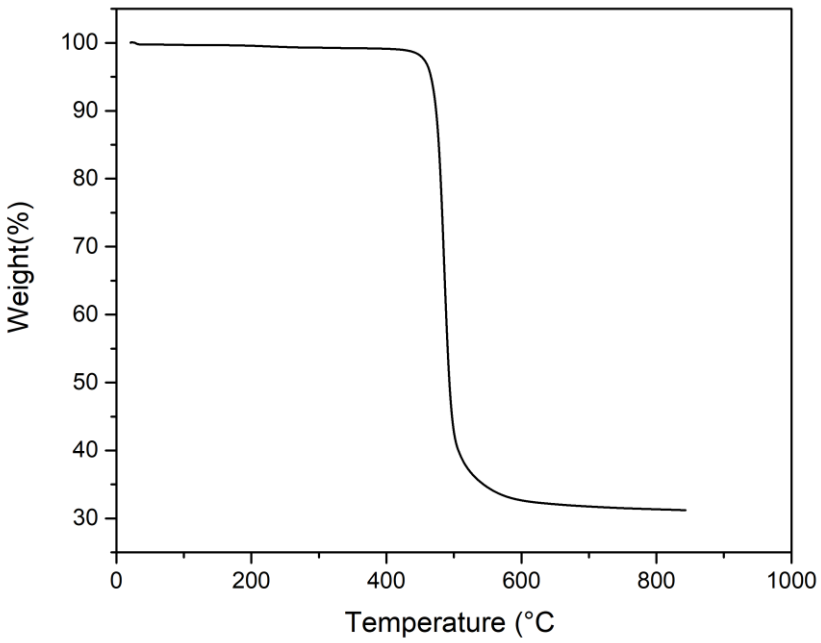

Figure 3.2 Thermogravimetric curve of parylene C.

doi:10.6342/NTU202301165

Since carbon would exist in many forms of allotropes, it was significant to identify chemical and physical properties of carbon. To characterize carbon-based materials, Raman spectroscopy was a versatile analysis tool[40]. In Figure 3.3, it showed the Raman spectrum of parylene C before and after carbonization. It was distinctively to see the change of characteristic peaks for parylene C during pyrolysis process. For example, the C-Cl stretching (690 cm^{-1}) and C-H stretching vibrations (2800 ~3100 cm^{-1}) of aromatic rings of parylene C[41, 42, 43] were disappeared after pyrolysis process. Figure 3.3(b) was the typical Raman spectrum of amorphous carbon[44, 45]. In brief, G band (1580 ~ 1600 cm^{-1}) originated with the in-plane bond stretching from sp^2 sites of carbon, and D band (1350 cm^{-1}) represented the presence of disorder for perfect graphite and graphene[44]. One could use the intensity ratio of D band and G band, I_D/I_G, to express the level of disorder in graphene[46].

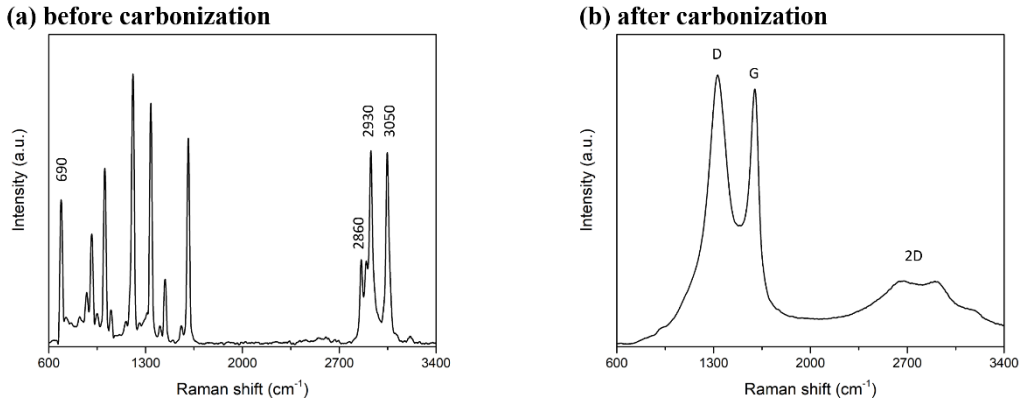

Figure 3.3 Raman spectrum of parylene C (a) before carbonization and (b) after carbonization.

doi:10.6342/NTU202301165

To investigate the variation of crystalline structure for parylene C during pyrolysis process, we did X-ray diffraction (XRD) measurements. In Figure 3.4 (a), there was a sharp peak at 2θ=14°, which came from the semi-crystalline structure of parylene C[47]. After pyrolysis, this crystalline structure was destroyed, turning into an amorphous material, which featured for its broad peak. Figure 3.4 (b) was the typical XRD result of amorphous carbon, which was characterized for its broad peak at 2θ=24°.[48]

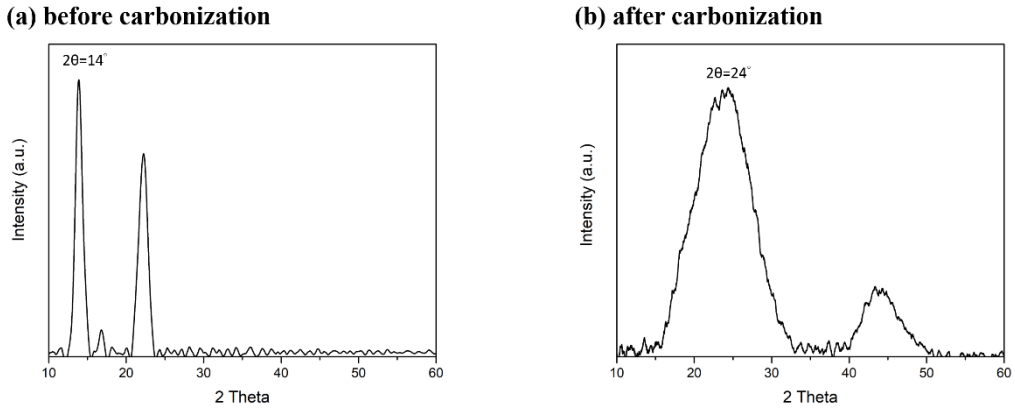

Figure 3.4 XRD results of parylene C (a) before carbonization and (b) after carbonization.

The above material characterization indicated parylene C had been successfully transformed into carbon. However, Raman spectroscopy and X-ray diffraction were solely the evidence of successful carbonization on the basis of physical and chemical properties. In the next section, we would do surface imaging to know whether the morphology has changed or whether the structure has maintained its integrity during the pyrolysis process.

doi:10.6342/NTU202301165

3.1.2 Morphology change

We have done surface imaging for two types of parylene sample, dense parylene film coating and porous parylene, respectively. For dense film coating type of parylene, the change of film thickness before and after carbonization was measured with AFM. Figure 3.5 showed the thickness of dense film coating decreased from 462 nm to 60 nm, which was relevant to the literature[42]. Thickness change could be corresponding to volume change, and the decreased volume was furtherly due to the loss of mass during pyrolysis process. Consequently, it could be a possible synthesis route to have multi-layer graphene on substrates with curved structures and complex geometries. On the basis of excellent control of ultra-thin film coating, it was probably achievable to have a few layers of carbon atom left on the substrate by pyrolysis process.

(a) before carbonization

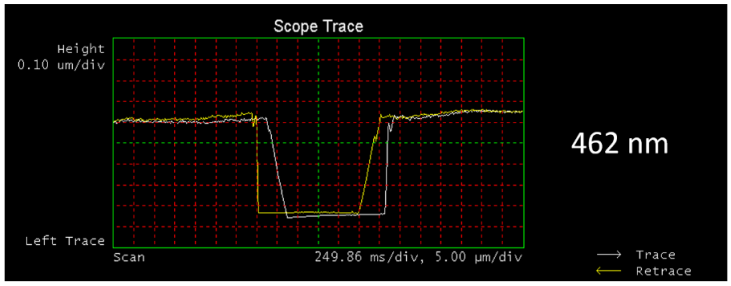

(b) after carbonization

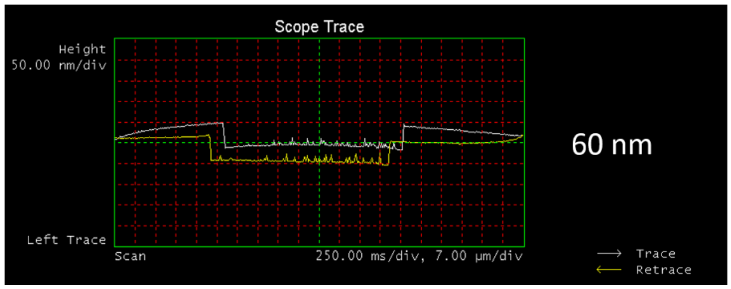

Figure 3.5 Thickness of dense film coating parylene (a) before carbonization and (b) after carbonization, measured with AFM.

doi:10.6342/NTU202301165

For porous parylene, we observed obvious shrinkage problem of porous structure and macroscopic morphology change during pyrolysis process. Figure 3.6 (a) showed the porous structure of parylene before carbonization by SEM. The scale of pore diameter was about 10~50 um. The morphology of the pore structure was in a shape of bead-like, which came from the vapor-phase polymerization and water vapor sublimation process. Figure 3.6 (b) indicated polymer-derived carbon having a distinct morphology difference between the original polymer porous structure. Compared with the original morphology, it was apparent to see smooth surface and the diminished pores. The reason for morphology change could be explained by the above introduced mechanism, coking. The morphology could not be preserved due to glass transition temperature (T_g) far lower than the heating temperature[49]. Parylene would flow like a semi-solid liquid because its T_g point was only about 100℃. Figure 3.6 (b) was the evidence of going through rubbery state for porous parylene, explaining the reason of oil-like surface. It was noted that the samples in Figure 3.6 were prepared from pure water ice-template and the following CVD process.

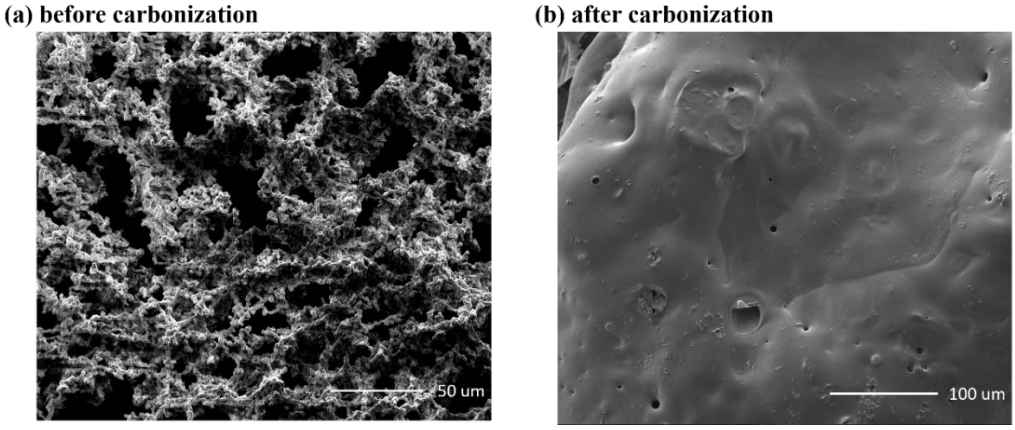

Figure 3.6 SEM images for (a) porous parylene before carbonization and (b) porous carbon from porous parylene after carbonization.

doi:10.6342/NTU202301165

So far, we have known what problems occurred during carbonization process. First, from results of TGA and AFM, there was a mass loss of polymer due to release of volatile hydrocarbon gas during heating process. This would result in coking or charring. Next, we observed that parylene had gone through a rubbery state and the resultant oil-like surface by SEM imaging, which were features of the coking mechanism. Since the aim of this research was to fabricate a hierarchical porous carbon material via temporal bubble structure, we have also done 3D profile microscope imaging to examine whether the foam-like pattern could preserve after pyrolysis process. In Figure 3.7, it was clear to see all foam-like structures with ~100 um scale of pore diameters disappeared after carbonization process. Similarly, it was due to the coking mechanism. It was noted that the samples in Figure 3.7 were prepared from 0.1 wt% tween80 ice-template from bubble blowing and the following CVD process. There was no addition of laponite yet.

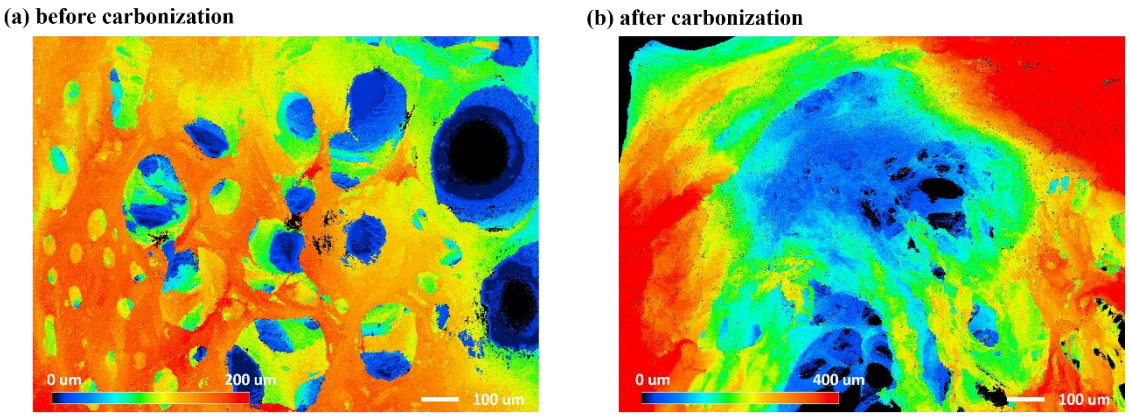

Figure 3.7 3D profile imaging of (a) porous parylene with foam structure before carbonization and (b) porous carbon from porous parylene with foam structure after carbonization. (addition of 0.1 wt% tween80)

doi:10.6342/NTU202301165

3.2 Structural integrity improvement

Concerning the shrinkage problem of polymer pattern, we used laponite RD^{R} (BYK, Germany) as an additive to provide stationary surface for flowing rubbery state of polymer during carbonization process. Laponite RD is a kind of artificial lithium magnesium silicate material. It is insoluble in water, but it can be well dispersive in aqueous solution, forming a highly shear-thinning gel. Giving from this particular and special property, it is common used in various application, such as emulsion, surface coating, and dermatological protection[50].

Samples in Figure 3.8 and Figure 3.9 were all prepared from solidified 1 wt% laponite ice-template. In Figure 3.8 (a), there was a pore structure because of two mechanisms. One was due to the competition process of vapor deposition and water sublimation. The other one was due to freeze drying process, leaving solid phase (laponite) as a structural framework[51]. The latter have the major contribution to this layered pore structure, giving that the morphology of porous parylene from pure ice-template was bead-like, not sheet-like. On the basis of excellent conformality of parylene, we could suppose that there was also a dense parylene film coating on the remained porous framework of laponite derived from freeze-drying mechanism. Figure 3.8 (b) and Figure 3.9 indicated that the pore structure preserved after carbonization process, showing improvement of structural integrity due to the laponite framework. Raman spectrum verified a conformal carbon layer on the laponite framework due to the carbonization of dense parylene film coating. Strictly speaking, there were still remained impurities in this porous carbon structure, which came from laponite. However, it was still acceptable to call it porous carbon if there was no side reaction or influence in the subsequent application, such as electrochemical catalysis, energy storage, and gas adsorption.

doi:10.6342/NTU202301165

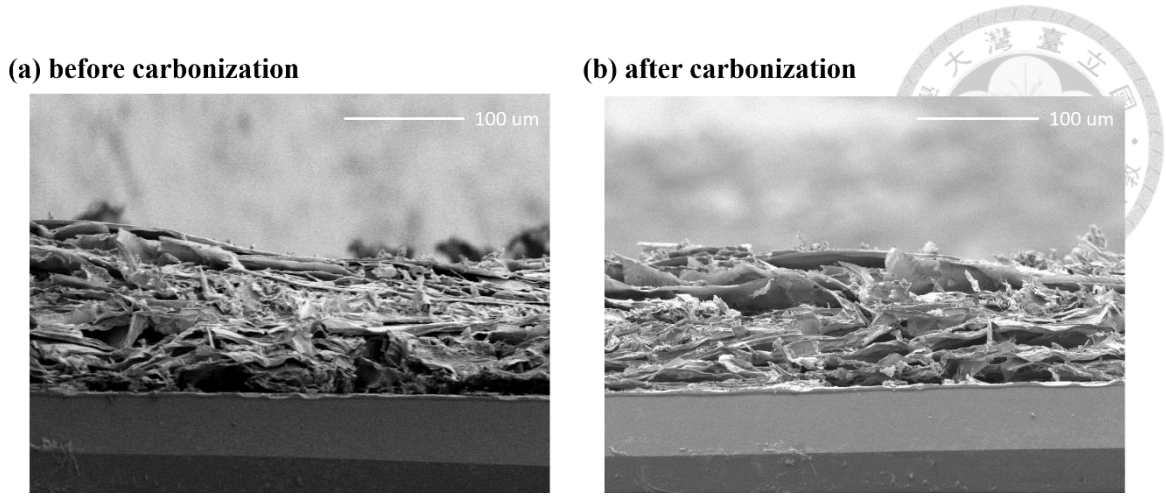

Figure 3.8 SEM of cross-section view of (a) porous parylene before carbonization and (b) porous carbon from porous parylene after carbonization. (addition of 1 wt% laponite)

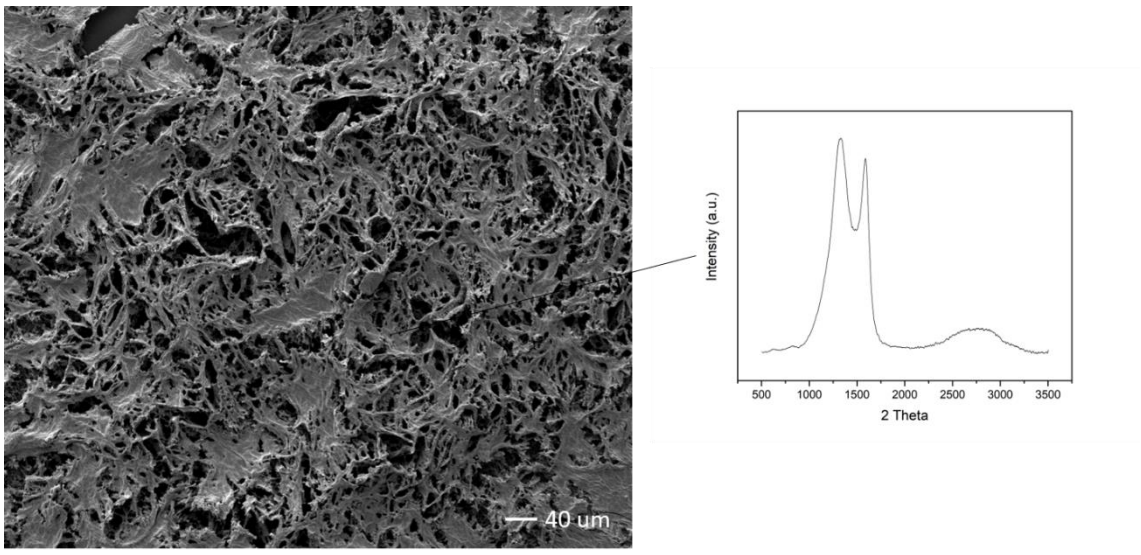

Figure 3.9 Raman spectrum and SEM of top view of porous carbon from porous parylene after carbonization. (addition of 1wt% laponite)

doi:10.6342/NTU202301165

3.3 Hierarchical porous structure

There are many researches focusing on the hierarchical porous carbon materials. By harnessing the benefits of numerous active sites found in micropores and the faster mass diffusion provided by mesopores, hierarchical porous carbon demonstrates improved electrochemical performance due to its synergistic effect of different pore sizes. However, most mature fabrication methods of hierarchical porous carbon are on the basis of template-assisted method, which is typically limited to either micropores or mesopores. When it comes to producing larger pore size up to hundreds of micrometers in scale, it seems time-consuming and environmentally hazardous by utilizing chemical agents for the removal of hard templates[52]. To overcome these challenges, this study presents a novel approach to synthesize hierarchical macroporous carbon materials, allowing for the tuning of pore sizes within the range of millimeters to centimeters.

3.3.1 Hierarchy structure

Figure 3.10 (a) illustrated the schematic representation of foam-like pore structure fabrication process. It was from the CVD process of temporal foam-like ice-template, followed by the carbonization process to get hierarchical porous carbon. Figure 3.10 (b) showed the highly tunable characteristic of primary pore size (um scale to cm scale). The cell window was from the original occupied space of air volume, forming the primary pore structure with larger pore size. On the other hand, the strut underwent a freeze-drying process, resulting in the formation of the secondary pore structure with smaller pore size (~10um). To validate the hierarchical structure could also maintain, we did SEM surface imaging for this porous parylene with foam structure after carbonization. Figure 3.10 (b) indicated both macroscopic foam structure and microscopic foam structure maintained

doi:10.6342/NTU202301165

structural integrity. It was interesting to note that some bubble membrane at the cell window got preserved during the CVD process, resulting in the partially-open cell window. This structure might give rise in more complex and intricate controllability of flow resistivity[53]. After carbonization, the fully-open cell window foam structure and the partially-open cell window foam structure were also captured. This morphological difference offered an additional parameter to control the flow behavior in individual sections due to the versatile tortuosity of interconnected pores. For instance, if the quantities of fully-open cell window and partially-open cell window could be carefully controlled, and these structures could be precisely positioned at desired locations with the desired orientation, it might result in varying degrees of mass transportation efficiency. This technique holds great promise for controlling flow behavior and could find practical applications in drug release systems.

doi:10.6342/NTU202301165

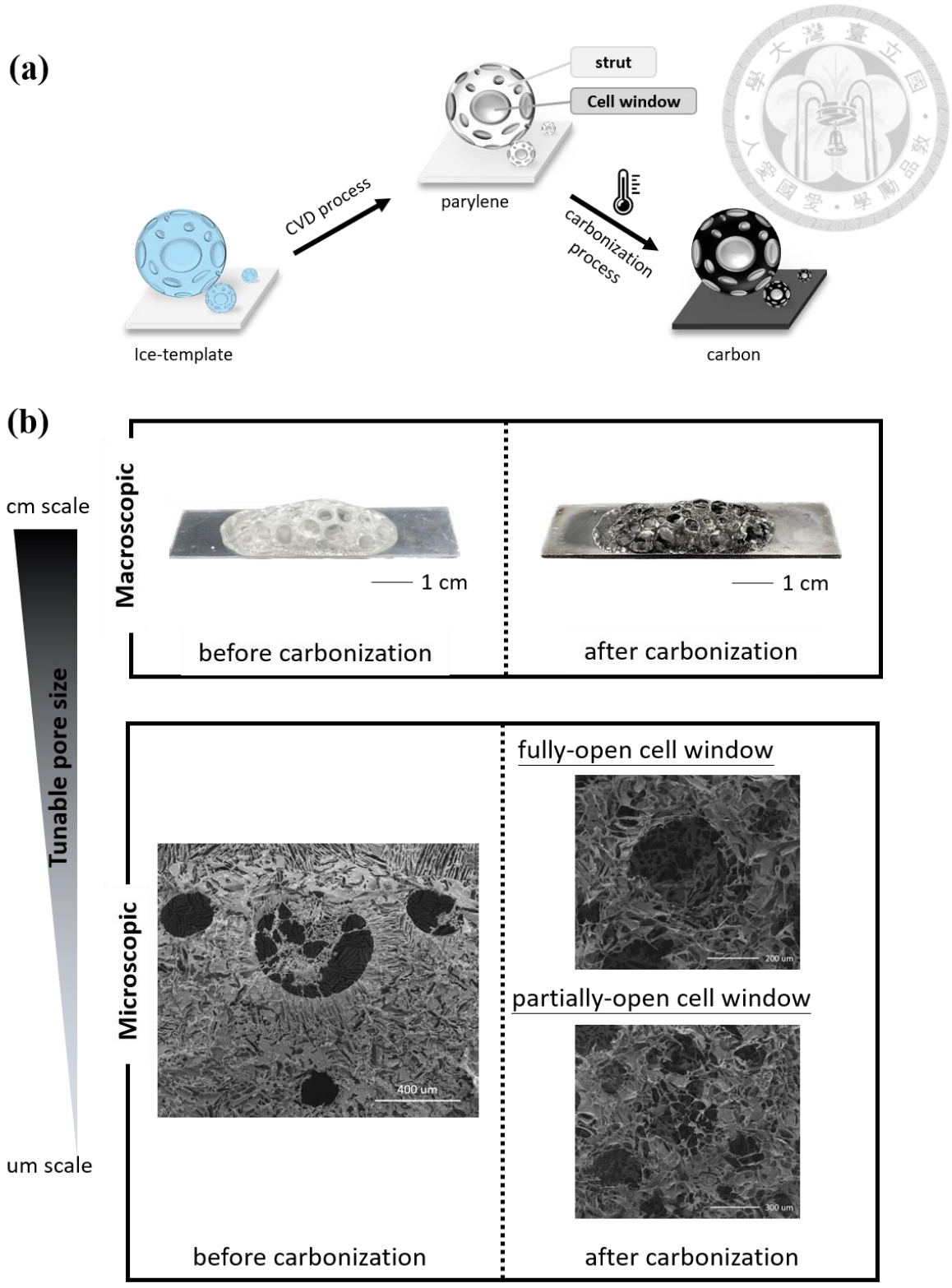

Figure 3.10 (a) Schematic representation of the hierarchical foam-like porous carbon structure. (b) Illustration of tunable primary pore size and structural integrity showed by SEM images. (addition of 0.1 wt% tween80 and 2% wt% laponite)

doi:10.6342/NTU202301165

3.3.2 Tunable morphology of foam-like structure

Hierarchical porous carbon material features with high specific surface area and efficient ion transportation. As a result, most fabrication methods were for micropores or mesopores. There is limited available research focusing on larger pore sizes up to the micrometer scales. It seems not an optimal choice starting from the hard-template method to produce larger pore sizes because of extended removal time for large sizes of hard-template particle. Differing from the encapsulation of solid materials using methods like the hard-template approach or the encapsulation of liquids like non-sublimated oil[54], this novel synthesis route offers a more convenient and easier way to fabricate porous materials with large pore size, simply on the basis of encapsulation of "air" by bubble. We have demonstrated the structural stability during heating process by addition of laponite. Consequently, pore size and geometry shape of the porous carbon could be controllable. Furthermore, the foam structure has versatile morphology. To emphasize the characteristics of highly tunable morphology of this approach, we showed a sample with interesting geometry and morphology as demonstration.

Figure 3.11 indicated a fractal structure, which was composed of main foam structure outside with larger pore size and secondary foam structure inside with smaller pore size, inside. The fractal-like structure could enhance its physical properties or tailored for specific applications[55]. For example[56], filters with varying porosity in depth are more effective at removing solute from a liquid than those with uniform porosity. This demonstration shed light on the advantage of tunable morphology, leading to variations in convection environments and fluid fields within the foam structure.

doi:10.6342/NTU202301165

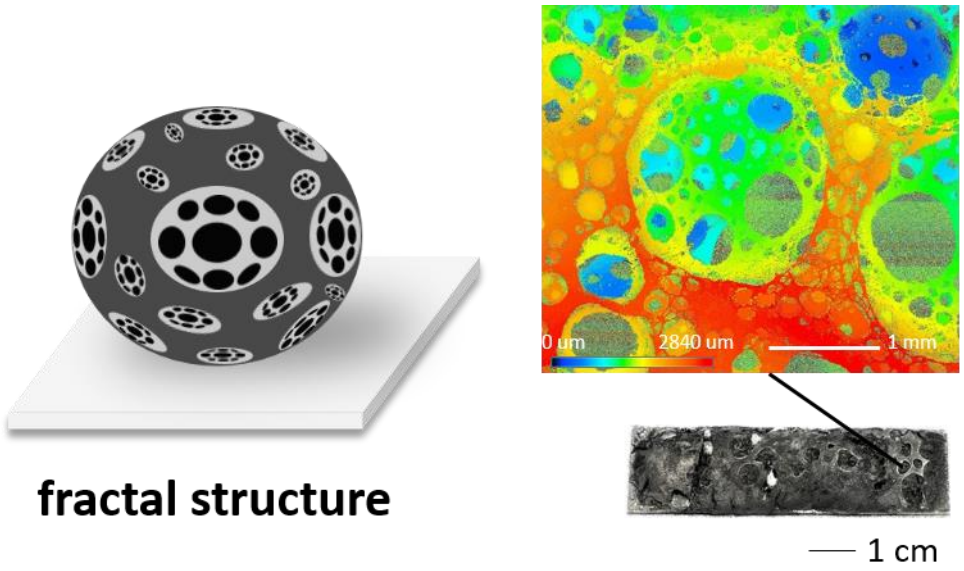

Figure 3.11 Tunable morphology illustration by fractal foam structure. (addition of 0.1 wt% tween80 and 2% wt% laponite)

doi:10.6342/NTU202301165

3.3.3 Thermal insulation test

Aerogel is a promising candidate for thermal insulation application thanks for its thermally super-insulating property [57]. According to the literature, aerogel can have thermal conductivity lower than that of still air[58], which makes it an important role in energy conservation. For example, it can be the substitute for windows, preventing additionally energy waste due to low-efficiency of the building envelope. Likewise, carbon aerogel is also famous for its outstanding thermal insulation property and excellent thermal stability, especially in ultrahigh-temperature environments[59, 60]. The total thermal conductivity can be separated into three components: gas conductivity, solid network conductivity and radiative conductivity. Given that the foam-like porous carbon structure proposed by this study is also a kind of carbon aerogel, we design a straightforward but interesting experiment to evaluate its thermal insulation performance.

The experiment setup is illustrated in Figure 3.12 (a). The ice cylinder has a volume of 1 mL and a diameter of 16 mm. The ice cylinder would be immersed into liquid nitrogen bath to make sure that the temperature of ice is 77 K. Each sample is in contact with the 373 K hotplate for a duration of 10 minutes to reach steady state. After achieving steady state, the ice cylinder would be set on the top surface of materials. The thermal insulation performance of materials is measured with required time for the completely melting of ice. The purpose of glass cap is to prevent the influence of force convection of air. There are three reasons for designing this experiment setup: (1) The use of thermal couples for measuring surface temperature poses challenges due to contact resistance issues, Additionally, it can potentially damage the material's structure, leading to difficulties in reproducing thermal insulation tests for the same sample. (2) The hotplate provides the stable heat flux to the material. To emphasize and highlight the significance

doi:10.6342/NTU202301165

of heat conduction through the material, the hotplate is set at a high temperature of 373 K. It would lower the contribution of heat flux from heat convection by air. (3) While not directly measuring the thermal conductivity values of each sample, this experiment indeed serves as a practical demonstration and application of thermal insulation.

Figure 3.12 (b) displayed the time required for melting of ice for the control, PDMS and fractal bubble structure carbon. Each sample utilized a 1 mm-thick quartz slide as a substrate, so the control sample consisted solely of the quartz slide itself. All samples had a consistent thickness of 3 mm. We took pure polydimethylsiloxane (PDMS) as a benchmark in the thermal insulation test due to its low thermal conductivity of only 0.16 W/mK[61]. The superior thermal insulation performance of the foam-like porous carbon compared to PDMS was evident, indicating the promising potential for thermal insulation applications.

Figure 3.12 (c) indicated the comparison of time required for completely melting of ice between foam-like porous structure and freeze-drying derived porous structure, with the examination of the impact of carbonization process. The variance in insulation performance between these two structures could be attributed to the increased convection-related problems resulting from the presence of cell windows with larger pore sizes, compared with pore sizes generated from the freeze-drying mechanism. Next, the time for melting ice had a minor change because of the carbonization process. Dense parylene film (with a thermal conductivity of k=0.084 W/mK) on the solid network changed into amorphous carbon (with a thermal conductivity ranging from k=3~10 W/mK) [62] after carbonization process. This change in thermal conductivity could potentially account for the minor change in the melting time.

doi:10.6342/NTU202301165

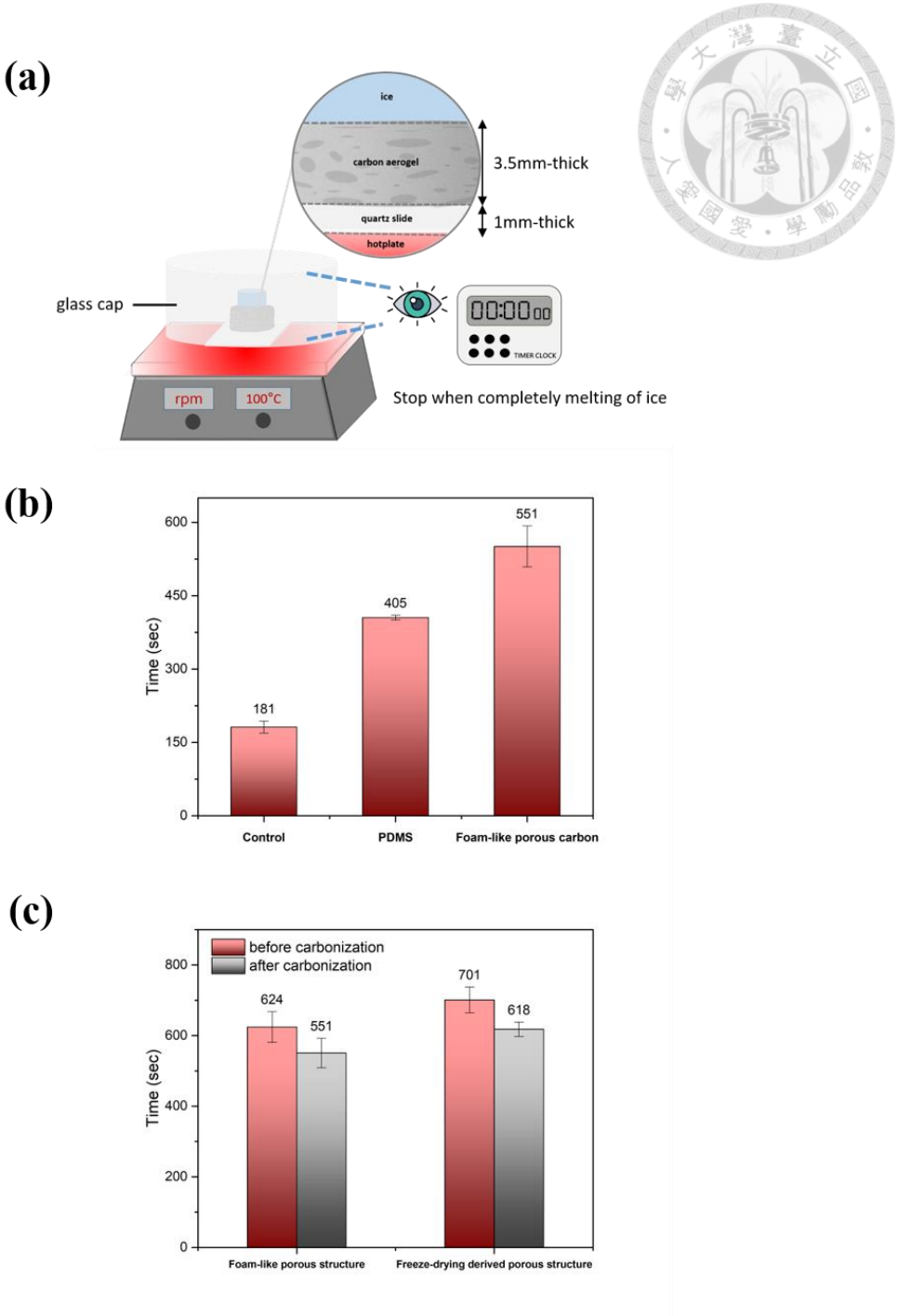

Figure 3.12 (a) Schematic illustration of thermal insulation experiment setup. (b) Time required for completely melting of ice for the control, PDMS and fractal bubble structure carbon. (c) Comparison of time required for completely melting of ice between foam-like porous structure and freeze-drying derived porous structure, with the examination of the impact of carbonization process.

doi:10.6342/NTU202301165

Chapter 4 Conclusion

4.1 Conclusion

Raman spectrum and X-ray diffraction spectrum confirmed the successful carbonization process of parylene. However, SEM images showed that there was a dramatic morphology change because of the coking mechanism. The TGA curve indicating the mass loss during pyrolysis process explained the change of film thickness measured with AFM before and after carbonization. As a result, we used the laponite to improve the structural integrity. Pore size and geometry shape of the porous carbon could be controllable. Given that most mature fabrication methods of hierarchical porous carbon were on the basis of template-assisted method, which was typically limited to either micropores or mesopores. It seemed time-consuming and environmentally hazardous by utilizing chemical agents for the removal of hard templates. As a result, we proposed a novel fabrication process for producing materials with larger pore size. It was from the CVD process of temporal foam-like ice-template. The cell window was from the original occupied space of air volume, forming the primary pore structure with ~100 um pore size. On the other hand, the strut underwent a freeze-drying process, resulting in the formation of the secondary pore structure with ~10 um pore size. To emphasize the characteristics of highly tunable morphology of this approach, we showed some samples with interesting geometry shapes and morphology as demonstration. The pore size of the cell window could reach sizes as large as centimeters. The fractal structure and the asymmetry structure were presented to show varying geometries.

Given that the foam-like porous carbon structure proposed by this study is also a kind of carbon aerogel, we designed a straightforward but interesting experiment to

doi:10.6342/NTU202301165

evaluate its thermal insulation performance. The superior thermal insulation performance of the foam-like porous carbon compared to PDMS was evident, indicating the promising potential for thermal insulation applications. The foam-like porous carbon would have convection-related problems resulting from the presence of cell windows with larger pore sizes. Besides, the carbonization of parylene into amorphous carbon accounted for the minor change in the thermal insulation performance.

4.2 Future work

This foam-like porous carbon is hierarchically macroporous at different length scales. As a result, it is not like conventional porous carbon having the feature of high specific surface area. To reach the goal of high specific surface area, micropores or mesopores have to be introduced into the material. Figure 4.1 reveals the BET surface area of pristine laponite and laponite annealed at 850°C. Since laponite has mesopores, intuitively, the first step is to use the etching agent to remove laponite to get the negative replica. However, the mesopores of laponite vanished due to the high heating temperature. As a result, there are two ways to achieve high specific surface area in the future work. The first approach is selecting others suitable inorganic materials as the structure framework while ensuring they maintain the intrinsic property of high specific surface area after pyrolysis process. The second approach involves implementing an activation process on the foam-like porous carbon to create micropores on its surface.

doi:10.6342/NTU202301165

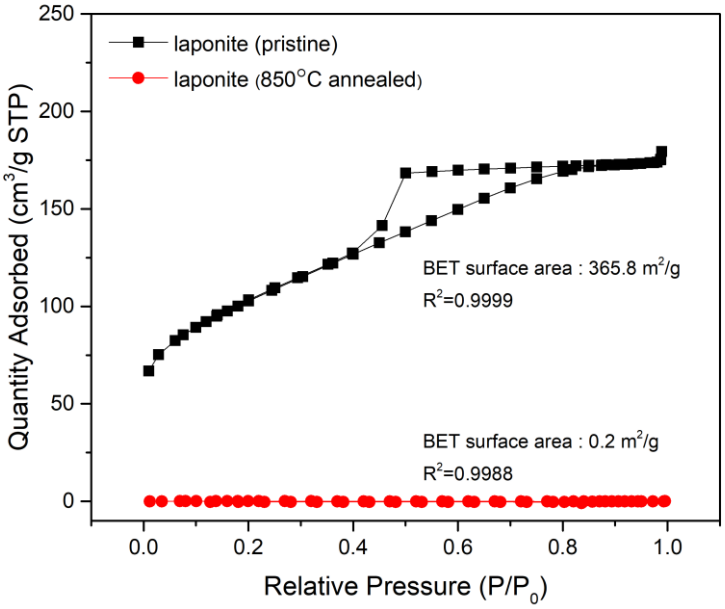

Figure 4.1 BET surface area of pristine laponite and laponite annealed at 850°C.

doi:10.6342/NTU202301165

Reference

(1) Thapliyal, V.; Alabdulkarim, M. E.; Whelan, D. R.; Mainali, B.; Maxwell, J. L. A concise review of the Raman spectra of carbon allotropes. *Diamond and Related Materials* **2022**, *127*, 109180. DOI: 10.1016/j.diamond.2022.109180.
(2) Schwander, M.; Partes, K. A review of diamond synthesis by CVD processes. *Diamond and Related Materials* **2011**, *20* (9), 1287-1301. DOI: 10.1016/j.diamond.2011.08.005.
(3) Mohan, V. B.; Lau, K.-t.; Hui, D.; Bhattacharyya, D. Graphene-based materials and their composites: A review on production, applications and product limitations. *Composites Part B: Engineering* **2018**, *142*, 200-220. DOI: 10.1016/j.compositesb.2018.01.013.
(4) Casari, C. S.; Milani, A. Carbyne: from the elusive allotrope to stable carbon atom wires. *MRS Communications* **2018**, *8* (2), 207-219. DOI: 10.1557/mrc.2018.48 From Cambridge University Press Cambridge Core.
(5) Acquah, S. F. A.; Penkova, A. V.; Markelov, D. A.; Semisalova, A. S.; Leonhardt, B. E.; Magi, J. M. Review—The Beautiful Molecule: 30 Years of C60 and Its Derivatives. *ECS Journal of Solid State Science and Technology* **2017**, *6* (6), M3155. DOI: 10.1149/2.0271706jss.
(6) Younis, M. R.; He, G.; Lin, J.; Huang, P. Recent Advances on Graphene Quantum Dots for Bioimaging Applications. *Frontiers in Chemistry* **2020**, *8*, Review. DOI: 10.3389/fchem.2020.00424.
(7) Xu, Q.; Li, W.; Ding, L.; Yang, W.; Xiao, H.; Ong, W.-J. Function-driven engineering of 1D carbon nanotubes and 0D carbon dots: mechanism, properties and applications. *Nanoscale* **2019**, *11* (4), 1475-1504, 10.1039/C8NR08738E. DOI: 10.1039/C8NR08738E.
(8) Kirchner, E.-M.; Hirsch, T. Recent developments in carbon-based two-dimensional materials: synthesis and modification aspects for electrochemical sensors. *Microchimica Acta* **2020**, *187* (8), 441. DOI: 10.1007/s00604-020-04415-3.
(9) Sun, Z.; Fang, S.; Hu, Y. H. 3D Graphene Materials: From Understanding to Design and Synthesis Control. *Chemical Reviews* **2020**, *120* (18), 10336-10453. DOI: 10.1021/acs.chemrev.0c00083.
(10) Feng, J.; Zheng, D.; Gao, X.; Que, W.; Shi, W.; Liu, W.; Wu, F.; Cao, X. Three-Dimensional Ordered Porous Carbon for Energy Conversion and Storage Applications. *Frontiers in Energy Research* **2020**, *8*, Mini Review. DOI: 10.3389/fenrg.2020.00210.
(11) Bianco, A.; Cheng, H.-M.; Enoki, T.; Gogotsi, Y.; Hurt, R. H.; Koratkar, N.; Kyotani, T.; Monthioux, M.; Park, C. R.; Tascon, J. M. D.; et al. All in the graphene family – A recommended nomenclature for two-dimensional carbon materials. *Carbon* **2013**, *65*, 1-6. DOI: 10.1016/j.carbon.2013.08.038.
(12) Pavlenko, V.; Khosravi H, S.; Żółtowska, S.; Haruna, A. B.; Zahid, M.; Mansurov, Z.; Supiyeva, Z.; Galal, A.; Ozoemena, K. I.; Abbas, Q.; et al. A comprehensive review of template-assisted porous carbons: Modern preparation methods and advanced applications. *Materials Science and Engineering: R: Reports* **2022**, *149*, 100682. DOI: 10.1016/j.mser.2022.100682.
(13) Wu, L.; Li, Y.; Fu, Z.; Su, B. L. Hierarchically structured porous materials: synthesis strategies and applications in energy storage. *Natl Sci Rev* **2020**, *7* (11), 1667-1701. DOI:

doi:10.6342/NTU202301165

10.1093/nsr/nwaa183 From NLM.
(14) Xia, Y.; Yang, Z.; Mokaya, R. Templated nanoscale porous carbons. *Nanoscale* **2010**, *2 5*, 639-659.
(15) Wang, C.; Yan, B.; Zheng, J.; Feng, L.; Chen, Z.; Zhang, Q.; Liao, T.; Chen, J.; Jiang, S.; Du, C.; et al. Recent progress in template-assisted synthesis of porous carbons for supercapacitors. *Advanced Powder Materials* **2022**, *1* (2), 100018. DOI: 10.1016/j.apmate.2021.11.005.
(16) Xiang, Y.; Lu, L.; Kottapalli, A. G. P.; Pei, Y. Status and perspectives of hierarchical porous carbon materials in terms of high-performance lithium–sulfur batteries. *Carbon Energy* **2022**, *4* (3), 346-398. DOI: 10.1002/cey2.185.
(17) Luo, X.; Chen, S.; Hu, T.; Chen, Y.; Li, F. Renewable biomass-derived carbons for electrochemical capacitor applications. *SusMat* **2021**, *1* (2), 211-240. DOI: 10.1002/sus2.8.
(18) Heidarinejad, Z.; Dehghani, M. H.; Heidari, M.; Javedan, G.; Ali, I.; Sillanpää, M. Methods for preparation and activation of activated carbon: a review. *Environmental Chemistry Letters* **2020**, *18* (2), 393-415. DOI: 10.1007/s10311-019-00955-0.
(19) Lee, J.-H.; Park, S.-J. Recent advances in preparations and applications of carbon aerogels: A review. *Carbon* **2020**, *163*, 1-18. DOI: 10.1016/j.carbon.2020.02.073.
(20) Enterría, M.; Figueiredo, J. L. Nanostructured mesoporous carbons: Tuning texture and surface chemistry. *Carbon* **2016**, *108*, 79-102. DOI: 10.1016/j.carbon.2016.06.108.
(21) Fu, R.-w.; Li, Z.-h.; Liang, Y.-r.; Li, F.; Xu, F.; Wu, D.-c. Hierarchical porous carbons: design, preparation, and performance in energy storage. *New Carbon Materials* **2011**, *26* (3), 171-179. DOI: 10.1016/S1872-5805(11)60074-7.
(22) Zhang, L.; Yang, X.; Zhang, F.; Long, G.; Zhang, T.; Leng, K.; Zhang, Y.; Huang, Y.; Ma, Y.; Zhang, M.; et al. Controlling the Effective Surface Area and Pore Size Distribution of sp2 Carbon Materials and Their Impact on the Capacitance Performance of These Materials. *Journal of the American Chemical Society* **2013**, *135* (15), 5921-5929. DOI: 10.1021/ja402552h.
(23) Seymour, J. P.; Elkasabi, Y. M.; Chen, H.-Y.; Lahann, J.; Kipke, D. R. The insulation performance of reactive parylene films in implantable electronic devices. *Biomaterials* **2009**, *30* (31), 6158-6167. DOI: 10.1016/j.biomaterials.2009.07.061.
(24) Valle, J. d.; Oliva, N. d. l.; Müller, M.; Stieglitz, T.; Navarro, X. Biocompatibility evaluation of parylene C and polyimide as substrates for peripheral nerve interfaces. In *2015 7th International IEEE/EMBS Conference on Neural Engineering (NER)*, 22-24 April 2015, 2015; pp 442-445. DOI: 10.1109/NER.2015.7146654.
(25) Humphrey, B. J. The Application of Parylene Conformal Coating Technology to Archival and Artifact Conservation. *Studies in Conservation* **1984**, *29* (3), 117-123. DOI: 10.2307/1506013 (acccessed 2023/04/20/).JSTOR.
(26) Gorham, W. F. A New, General Synthetic Method for the Preparation of Linear Poly-p-xylylenes. *Journal of Polymer Science Part A-1: Polymer Chemistry* **1966**, *4* (12), 3027-3039, DOI: 10.1002/pol.1966.150041209 (acccessed 2023/04/18).
(27) Fortin, J. B.; Lu, T. M. A Model for the Chemical Vapor Deposition of Poly(para-xylylene) (Parylene) Thin Films. *Chemistry of Materials* **2002**, *14* (5), 1945-1949. DOI: 10.1021/cm010454a.
(28) Tung, H.-Y.; Sun, T.-P.; Sun, H.-Y.; Guan, Z.-Y.; Hu, S.-K.; Chao, L.; Chen, H.-Y. Construction and control of 3D porous structure based on vapor deposition on sublimation solids. *Applied Materials Today* **2017**, *7*, 77-81. DOI: 10.1016/j.apmt.2016.12.005.

doi:10.6342/NTU202301165

(29) Chang, Y.-M.; Xiao, J.-Q.; Christy, J.; Wu, C.-Y.; Huang, C.-W.; Wu, T.-Y.; Chiang, Y.-C.; Lin, T.-H.; Chen, H.-Y. Ice-templated synthesis of multicomponent porous coatings via vapour sublimation and deposition polymerization. *Materials Today Bio* **2022**, *16*, 100403. DOI: 10.1016/j.mtbio.2022.100403.
(30) Liu, Y.; Kang, D.; Dai, W.; Li, H.; Wang, W.; Tai, Y.-C. Highly controllable and reliable ultra-thin Parylene deposition. *Micro and Nano Systems Letters* **2018**, *6* (1), 5. DOI: 10.1186/s40486-018-0067-0.
(31) Ullah, S.; Yang, X.; Ta, H. Q.; Hasan, M.; Bachmatiuk, A.; Tokarska, K.; Trzebicka, B.; Fu, L.; Rummeli, M. H. Graphene transfer methods: A review. *Nano Research* **2021**, *14* (11), 3756-3772. DOI: 10.1007/s12274-021-3345-8.
(32) Forouzanfar, S.; Pala, N.; Madou, M.; Wang, C. Perspectives on C-MEMS and C-NEMS biotech applications. *Biosensors and Bioelectronics* **2021**, *180*, 113119. DOI: 10.1016/j.bios.2021.113119.
(33) Richa, A.; Majid, B.; Wei, C.; Chunlei, W. Carbon microelectromechanical systems (C-MEMS) based microsupercapacitors. In *Proc.SPIE*, 2015; Vol. 9493, p 94930C. DOI: 10.1117/12.2180122.
(34) Oberlin, A. Carbonization and graphitization. *Carbon* **1984**, *22* (6), 521-541. DOI: 10.1016/0008-6223(84)90086-1.
(35) Natu, R.; Islam, M.; Gilmore, J.; Martinez-Duarte, R. Shrinkage of SU-8 microstructures during carbonization. *Journal of Analytical and Applied Pyrolysis* **2018**, *131*, 17-27. DOI: 10.1016/j.jaap.2018.02.015.
(36) Jenkins, G. M.; Kawamura, K. *Polymeric carbons: carbon fibre, glass and char*; Cambridge University Press, 1976.
(37) Sharma, S. Glassy Carbon: A Promising Material for Micro- and Nanomanufacturing. In *Materials*, 2018; Vol. 11.
(38) Joesten, B. L. Thermogravimetry and differential scanning calorimetry of some poly-p-xylylenes containing halogen atoms. *Journal of Applied Polymer Science* **1974**, *18* (2), 439-448. DOI: 10.1002/app.1974.070180211.
(39) Sharma, S.; Rostas, A. M.; Bordonali, L.; MacKinnon, N.; Weber, S.; Korvink, J. G. Micro and nano patternable magnetic carbon. *Journal of Applied Physics* **2016**, *120* (23). DOI: 10.1063/1.4972476 (acccessed 4/21/2023).
(40) Wu, J.-B.; Lin, M.-L.; Cong, X.; Liu, H.-N.; Tan, P.-H. Raman spectroscopy of graphene-based materials and its applications in related devices. *Chemical Society Reviews* **2018**, *47* (5), 1822-1873, 10.1039/C6CS00915H. DOI: 10.1039/C6CS00915H.
(41) Yang, M.; Jeong, S. W.; Chang, S. J.; Kim, K. H.; Jang, M.; Kim, C. H.; Bae, N. H.; Sim, G. S.; Kang, T.; Lee, S. J.; et al. Flexible and Disposable Sensing Platforms Based on Newspaper. *ACS Applied Materials & Interfaces* **2016**, *8* (51), 34978-34984. DOI: 10.1021/acsami.6b10298.
(42) Song, Z.; Park, J.-H.; Kim, H.-R.; Lee, G.-Y.; Kang, M.-J.; Kim, M.-H.; Pyun, J.-C. Carbon electrode obtained via pyrolysis of plasma-deposited parylene-C for electrochemical immunoassays. *Analyst* **2022**, *147* (16), 3783-3794, 10.1039/D2AN00854H. DOI: 10.1039/D2AN00854H.
(43) Mathur, M. S.; Weir, N. A. Laser raman and infrared spectrum of poly-p-xylylene. *Journal of Molecular Structure* **1973**, *15* (3), 459-463. DOI: 10.1016/0022-2860(73)80016-X.
(44) Ferrari, A. C.; Robertson, J. Interpretation of Raman spectra of disordered and amorphous carbon. *Physical Review B* **2000**, *61* (20), 14095-14107. DOI:

doi:10.6342/NTU202301165

10.1103/PhysRevB.61.14095.
(45) Lin, J.; Peng, Z.; Liu, Y.; Ruiz-Zepeda, F.; Ye, R.; Samuel, E. L. G.; Yacaman, M. J.; Yakobson, B. I.; Tour, J. M. Laser-induced porous graphene films from commercial polymers. *Nature Communications* **2014**, *5* (1), 5714. DOI: 10.1038/ncomms6714.
(46) Childres, I.; Jauregui, L. A.; Park, W.; Cao, H.; Chen, Y. P. Raman spectroscopy of graphene and related materials. *New developments in photon and materials research* **2013**, *1*.
(47) Hsu, J.-M.; Rieth, L. W.; Kammer, S.; Orthner, M. P.; Solzbacher, F. Effect of thermal and deposition processes on surface morphology, crystallinity, and adhesion of Parylene-C. *Sensors and Materials* **2008**, *20*, 87-102.
(48) Rajan, A. S.; Sampath, S.; Shukla, A. K. An in situ carbon-grafted alkaline iron electrode for iron-based accumulators. *Energy & Environmental Science* **2014**, *7* (3), 1110-1116, 10.1039/C3EE42783H. DOI: 10.1039/C3EE42783H.
(49) Zakhurdaeva, A.; Dietrich, P.-I.; Hölscher, H.; Koos, C.; Korvink, J. G.; Sharma, S. Custom-Designed Glassy Carbon Tips for Atomic Force Microscopy. *Micromachines* **2017**, *8* (9), 285.
(50) Tomás, H.; Alves, C. S.; Rodrigues, J. Laponite®: A key nanoplatform for biomedical applications? *Nanomedicine* **2018**, *14* (7), 2407-2420. From NLM.
(51) Shao, G.; Hanaor, D. A. H.; Shen, X.; Gurlo, A. Freeze Casting: From Low-Dimensional Building Blocks to Aligned Porous Structures—A Review of Novel Materials, Methods, and Applications. *Advanced Materials* **2020**, *32* (17), 1907176. DOI: 10.1002/adma.201907176.
(52) Ghaedi, H.; Zhao, M. Review on Template Removal Techniques for Synthesis of Mesoporous Silica Materials. *Energy & Fuels* **2022**, *36* (5), 2424-2446. DOI: 10.1021/acs.energyfuels.1c04435.
(53) Yu, X.; Lu, Z.; Zhai, W. Enhancing the flow resistance and sound absorption of open-cell metallic foams by creating partially-open windows. *Acta Materialia* **2021**, *206*, 116666. DOI: 10.1016/j.actamat.2021.116666.
(54) Chiu, Y.-R.; Hsu, Y.-T.; Wu, C.-Y.; Lin, T.-H.; Yang, Y.-Z.; Chen, H.-Y. Fabrication of Asymmetrical and Gradient Hierarchy Structures of Poly-p-xylylenes on Multiscale Regimes Based on a Vapor-Phase Sublimation and Deposition Process. *Chemistry of Materials* **2020**, *32* (3), 1120-1130. DOI: 10.1021/acs.chemmater.9b04047.
(55) Lakes, R. Materials with structural hierarchy. *Nature* **1993**, *361* (6412), 511-515. DOI: 10.1038/361511a0.
(56) Dalwadi, M. P.; Griffiths, I. M.; Bruna, M. Understanding how porosity gradients can make a better filter using homogenization theory. *Proceedings of the Royal Society A: Mathematical, Physical and Engineering Sciences* **2015**, *471* (2182), 20150464. DOI: 10.1098/rspa.2015.0464.
(57) Fu, Z.; Corker, J.; Papathanasiou, T.; Wang, Y.; Zhou, Y.; Madyan, O. A.; Liao, F.; Fan, M. Critical review on the thermal conductivity modelling of silica aerogel composites. *Journal of Building Engineering* **2022**, *57*, 104814. DOI: 10.1016/j.jobe.2022.104814.
(58) Abraham, E.; Cherpak, V.; Senyuk, B.; ten Hove, J. B.; Lee, T.; Liu, Q.; Smalyukh, I. I. Highly transparent silanized cellulose aerogels for boosting energy efficiency of glazing in buildings. *Nature Energy* **2023**, *8* (4), 381-396. DOI: 10.1038/s41560-023-01226-7.
(59) Wiener, M.; Reichenauer, G.; Braxmeier, S.; Hemberger, F.; Ebert, H. P. Carbon

doi:10.6342/NTU202301165

Aerogel-Based High-Temperature Thermal Insulation. *International Journal of Thermophysics* **2009**, *30* (4), 1372-1385. DOI: 10.1007/s10765-009-0595-1.
(60) Zhang, H.; Feng, J.; Li, L.; Jiang, Y.; Feng, J. Preparation of a carbon fibre-reinforced carbon aerogel and its application as a high-temperature thermal insulator. *RSC Advances* **2022**, *12* (22), 13783-13791, 10.1039/D2RA00276K. DOI: 10.1039/D2RA00276K.
(61) Wei, J.; Liao, M.; Ma, A.; Chen, Y.; Duan, Z.; Hou, X.; Li, M.; Jiang, N.; Yu, J. Enhanced thermal conductivity of polydimethylsiloxane composites with carbon fiber. *Composites Communications* **2020**, *17*, 141-146. DOI: 10.1016/j.coco.2019.12.004.
(62) Giri, A.; Dionne, C. J.; Hopkins, P. E. Atomic coordination dictates vibrational characteristics and thermal conductivity in amorphous carbon. *npj Computational Materials* **2022**, *8* (1), 55. DOI: 10.1038/s41524-022-00741-7.

doi:10.6342/NTU202301165

Appendix

口試提問

Q1: 此結構是類似 carbon areogel 的概念嗎?可以透過改變孔洞大小或更緻密結構影響絕熱效果嗎?

A1: 都是同屬於利用孔洞材料中的空氣來當作絕熱手段，孔洞大小或孔隙率等材料結構上的變化都會影響絕熱效果。

Q2: 是否量測過孔洞機制，可不可以稱作 aerogel?

A2: 沒有量測過，根據實驗室以往的數據，這個孔洞材料的孔隙率可能大約是60~70%，與一般 aerogel 的定義 99.98%孔隙率仍有差距。

Q3: 碳的結構如何鑑定?如何知道碳鏈的排列方式。

A3: 可以簡單從 Raman 光譜中的 D band、G band，或者是從 XPS 儀器鑑定，來推測碳的 sp^2 軌域、sp^3 軌域各自的占比是多少。

Q4: 絕熱方面來看，aerogel 和較導熱的碳互相矛盾，為何不用原來的 porous structure?

A4: Carbon aerogel 可以承受更高溫的環境，在高溫環境下不會像高分子類的 aerogel 有軟化的現象。

Q5: 測絕熱的環境溫度是多少，有沒有測過更高溫的?

A5: 目前是加熱板 100℃，有測試過 200℃ 的，但冰塊融化成水之後，流到加熱板上會有沸騰現象，導致孔洞材料被沸騰的水給沖壞。

Q6: 建議更精準方式測熱傳，熱像儀量測表面，整個環境都高溫，可能有誤差。

A6: 實驗上的確有許多因素會造成量測誤差，但若是每組樣品的待測環境都相同，

doi:10.6342/NTU202301165

控制變因都一樣的話，這個方式還是可以方便我們更直觀觀察到絕熱效果。

Q7: 結構脆的問題，要如何增加機械性質?

A7: 可以選用 carbon fiber 當作填充材。

Q8: 碳化後的薄膜結構如何量測?

A8: 使用 AFM 量測膜厚變化，可以觀察到膜厚變薄，與 TGA 數據相驗證。

doi:10.6342/NTU202301165